

Ochratoxin A Sensor Based on Nanocomposite Hybrid Film of Ionic Liquid-Graphene Nano-Sheets Using Coulometric FFT Cyclic Voltammetry

P. Norouzi^{1,2,*}, B. Larijani,^{2,*} M. R. Ganjali^{1,2}

¹ Center of Excellence in Electrochemistry, University of Tehran, Tehran, Iran

² Endocrinology & Metabolism Research Center, Tehran University of Medical Sciences, Tehran, Iran

*E-mail: norouzi@khayam.ut.ac.ir

Received: 28 June 2012 / Accepted: 23 July 2012 / Published: 1 August 2012

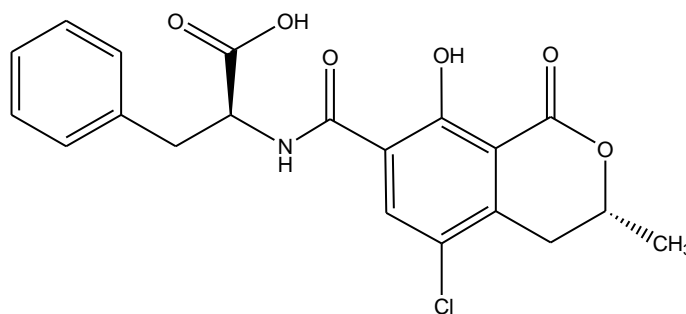
A new electrochemical method was introduced for determination of ochratoxin A, using fast Fourier transformation cyclic voltammetry (CFFTCV) combined with a novel electrochemical sensor. The sensor was designed based on reduction of gold nanoparticles on graphene nanosheets oxide hybrid with ionic liquid (1-butyl-3-methylimidazolium tetra fluoroborate) on the surface of a glassy carbon electrode. Also, in this method the response of the sensor was calculated in form of charge changes under the peak by integrated the current in selected potential range. The experimental conditions, for the electrochemical measurement were optimized. The linear concentrations range of OCA was from 1–200 nM with a detection limit of 2.2×10^{-10} M. Moreover, the proposed sensor exhibited good accuracy, short response time (less than 7s), high sensitivity with repeatability (R.S.D value of 2.5%) and long term stability (60 days with a decrease of 5.5% in response).

Keywords: FFT cyclic Voltammetry; Ochratoxin A; Gold nanoparticles; Graphene nanosheet; Ionic liquid

1. INTRODUCTION

Ochratoxin A, (OCA, Scheme 1) 7-(1- β -phenylalanylcarbonyl)-carboxyl-5-chloro-8-hydroxy-3,4-dihydro-3R-methylisocoumarin, is a coumarinic mycotoxin produced by *Aspergillus ochraceus*, *Aspergillus carbonarius* and *Penicillium verrucosum*. It is one of the most abundant food-contaminating toxins and can be found in a wide range of foods, stored food such as cereals, cocoa, coffee, dried fruit, and in meat products as a result of contamination of animal feed [1-4]. This mycotoxin is a powerful nephrotoxic, teratogenic, immunosuppressive agent and the International Agency for Research on Cancer (IARC) classified OCA in 2B Group (possibly carcinogenic agent)

[5]. The Commission Regulations (EU) has established the maximum levels for OCA in cereals of $5 \mu\text{g kg}^{-1}$, all products derived from cereals of $3 \mu\text{g kg}^{-1}$, processed cereal-based foods and baby-foods of $0.5 \mu\text{g kg}^{-1}$ [6,7]. In addition, OCA is also suspected to cause the Balkan Endemic Nephropathy in rural areas in South-Eastern Europe and urinary tract tumor. Due to health concerns, there is an increasing need for fast, reliable and low-cost analytical methods for monitoring OCA. Numerous methods for the determination of OCA have been reported including liquid chromatography (LC) [8], thin-layer chromatography (TLC) [9], gas chromatography (GC) [10], capillary electrophoresis (CE) [11] and enzyme-linked immunosorbent assay (ELISA) [12].



Scheme 1. Chemical structure of Ochratoxin A

In this work, a new electrochemical method is introduced for determination of OCA. The coulometric FFT cyclic voltammetry (CFFTCV) technique [13-30] combined with a new sensor was used for sensitive detection of OCA. The sensor was designed based on formation of gold nanoparticles on reduced graphene nanosheets oxide (RGNS) hybrid with ionic liquid, (1-butyl-3-methylimidazolium tetra fluoroborate) on a glassy carbon electrode surface. The presence of AuNPs and RGNS in modification of the electrode provides an environment that could enhance the electrocatalytic activities of the sensor. Scanning electron microscopy and impedance spectroscopy (EIS) was used to characterize the sensor surface.

2. MATERIALS AND METHODS

2.1. Reagents

Ochratoxine A, potassium ferricyanide, sodium chloride, potassium chloride, sodium phosphate dibasic (Na_2HPO_4), sulfuric acid (98%), ethanol (98%) were all purchased from Merck Co. 1-butyl-3-methylimidazolium tetrafluoroborate (BMIM- BF_4 , ionic liquid, IL) were of analytical grades from Merck. Graphene nanosheets (GNS) purchased from Sinopharm Henan Bonzer Imp. 0.05 M $\text{NaH}_2\text{PO}_4/\text{Na}_2\text{HPO}_4$ buffer solutions at pH 7.0 were used as the supporting electrolyte. The prepared solutions were kept at 4°C before use.

Graphene nanosheets oxide (GNSO) was synthesized from graphite through oxidization using NaNO_3 , H_2SO_4 , and KMnO_4 . Next, a 1.0 mg/mL solution was ultrasonicated for 1.5 h to form a claybank dispersion and was further reacted with 10.0 mL of hydrazine hydrate for 12 h under 95 °C. At the end, reduced GNS (RGNS) was filtrated collected and further washed with water.

2.2. The sensor preparation

A glassy carbon electrode, GCE, (3 mm in diameter) were polished well with 1.0, 0.3 and 0.05 μm alumina slurry and then it was washed thoroughly with doubly distilled water. The electrodes were successively sonicated in 1:1 nitric acid, acetone and doubly distilled water, and then allowed to dry at room temperature. For construction of IL-RGNS/GCE, GNSO suspension in ionic liquid (2-25 μL) was dropped onto the surface of the GCE. The GNSO film was electrochemically reduced in a phosphate buffer solution (PBS, pH 7.0) for 200 s at -1 V to form RGNS-IL /GCE.

Gold nanoparticles were then produced by reducing HAuCl_4 with sodium citrate at 100 °C for half an hour. The mean size of the prepared Au colloids was about 20-60 nm, estimated by transmission electron microscopy in a separate experiment. The prepared sensor was stored at 4 °C in PBS before use. The schematic diagram of the construction of the OCA sensor is shown in figure 1.

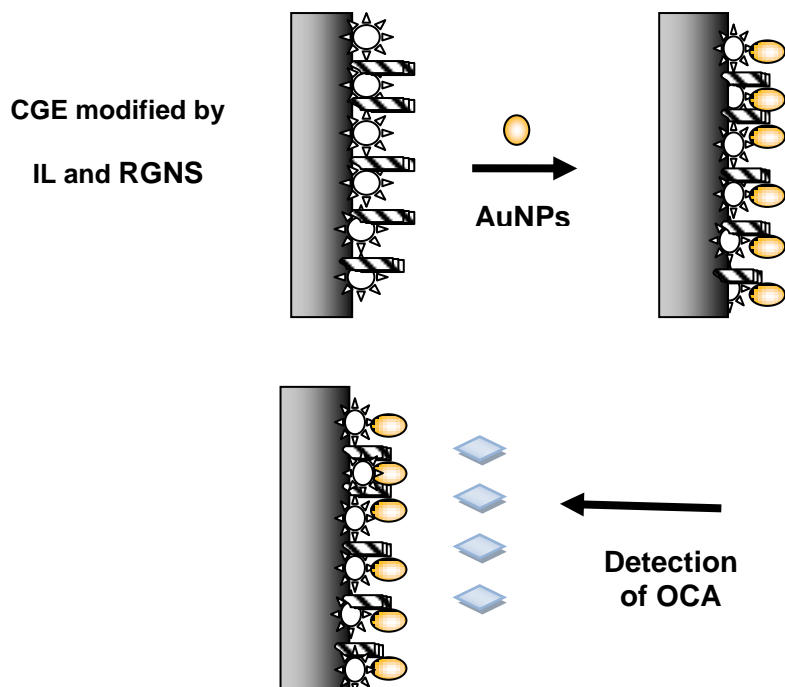


Figure 1. Schematic figures of the sensor preparation

2.3. Instrumentation and Data Acquisition and Processing

A homemade potentiostat was used for CFFTCV voltammetric measurements. The potentiostat was connected to a PC equipped with an analog to digital data acquisition board (PCL-818H, Advantech Co.). During the experiments, the computer was dictated by the condition for the data acquisition requirements electrochemical software was developed in Delphi 6.0 environment. The program was used to generate an analog waveform and acquire current readings. The potential waveform was, repeatedly, applied to the working electrode and then the data was acquired, and stored by the software. Also, the program was able to process and plot the data in real time.

EIS measurements were performed in 3 mM $K_3Fe(CN)_6$ in PBS at pH 7.0. A stock solution of 5 mM OCA was firstly prepared, and then an aliquot was diluted to the appropriate concentration. Before each measurement, the three-electrode system was installed in a blank solution, and the peak current voltammetry scan from -800 to 800 mV (vs. SCE) was recorded.

The sensor response, in this detection method, was based on the charge under peak in CVs. The unit for the resulted OCA signal however will change from ampere to coulomb (C), which is the charge changes (ΔQ) under the CV curve at a selected potential range, E_1 to E_2 .

The equation for biosensor response is

$$\Delta Q_n = \int_{E_1}^{E_2} \Delta i_{(n,E)} dE - ave \left[\int_{E_1}^{E_2} \Delta i_{(m,E)} dE \right] \quad \text{for } n > 0 \quad (1)$$

or

$$\Delta Q_n = Q_n - Q_{ave} \quad (2)$$

where Q_{ave} and Q_n are the calculated average charges at the selected potential range, E_1 to E_2 , from m CVs and the calculated charge at the same potential range from subsequent n^{th} cyclic voltammogram, respectively.

3. RESULTS AND DISCUSSION

Fig. 2A shows SEM image of the surface of the constructed sensor. In this figure, it could be seen that RGNS showed the typical crumpled structure, and the magnitude and distribution of AuNPs on the surface of RGNS/GCE were uniform. In fact, the composite surface is well-coated with AuNPs; the diameters of the NPs are 20–60 nm, while, the density of nanoparticles with diameters smaller than 30 nm is higher. This is reasonable to deduce that IL played an important role here. As suggested by other researchers, the nucleation rate is higher at ILs surface due to exist a low interfacial tension, and thus can enhance, which is favorable to the formation of smaller AuNPs. Homogeneity of the surface indicates that they are consisted of a homogeneous distribution of the materials.

Fig 2B shows EIS measurements results of the electrode at different stages of fabrication process, in 3.0 mM $[Fe(CN)_6]^{3-/4-}$ in 0.1 M KCl. In Randles circuit, it is assumed that resistance to

electron transfer and the diffusion impedance is parallel to the interfacial double layer capacitance. In this plot, the semicircle portion, observed at higher frequencies, corresponds to electron transfer limited process, whereas the linear part is characteristic of the lower frequencies range and represents the diffusion-limited electron-transfer process. It can be seen that in curve (a) for the bare GCE, the value of R_{et} was smaller than value shown in curve (b) for RGNS-IL/GCE. This indicates that the immobilization of the RGNS-IL induces an increase in the semi-circular diameter indicating an increase of the electron transfer resistance. However, after AuNPs deposited, the value of R_{et} decreased (curve c), which indicates that AuNPs and RGNS encompass excellent electrical conducting materials, which can enhance the electron transfer of $[Fe(CN)_6]^{3-/4-}$ at the surface of the electrode.

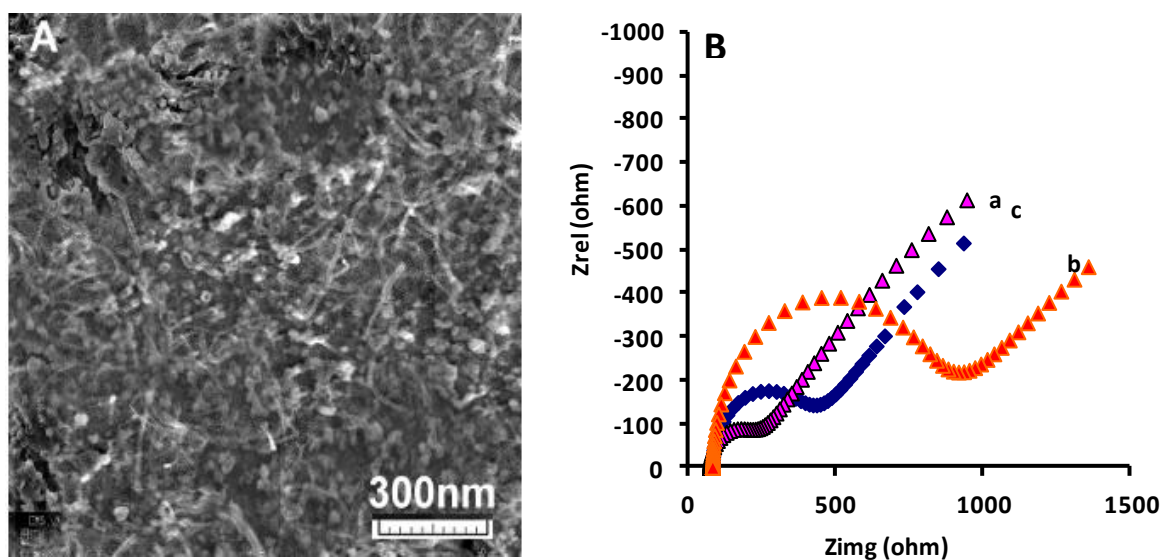
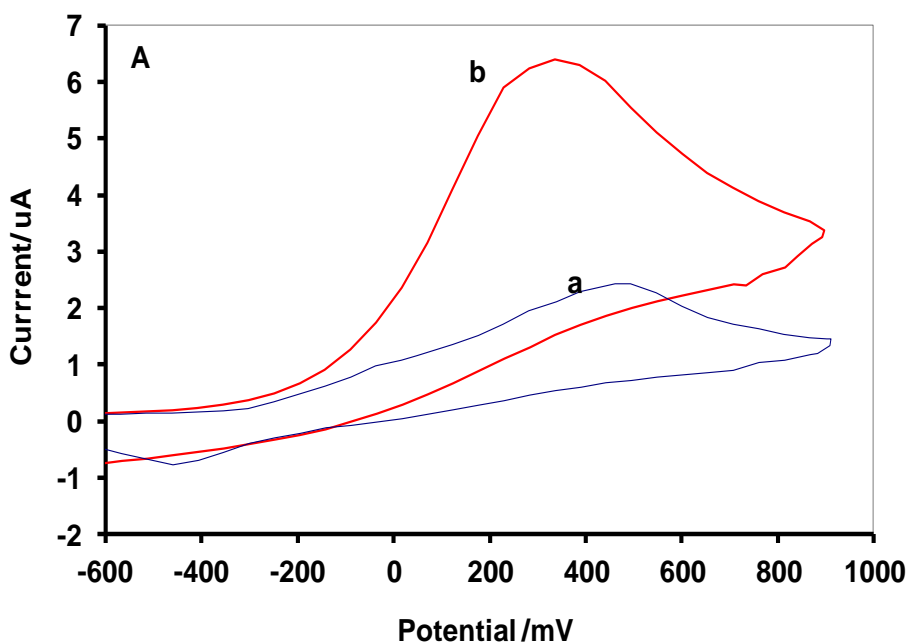


Figure 2. A) SEM images of the surface of the sensor. B) EIS plots of modified electrode in 3 mM $K_3Fe(CN)_6$ with 0.05 M KCl: (a) bare GCE (b) RGNS-IL/GCE and (c) AuNPs /RGNS-IL/GCE



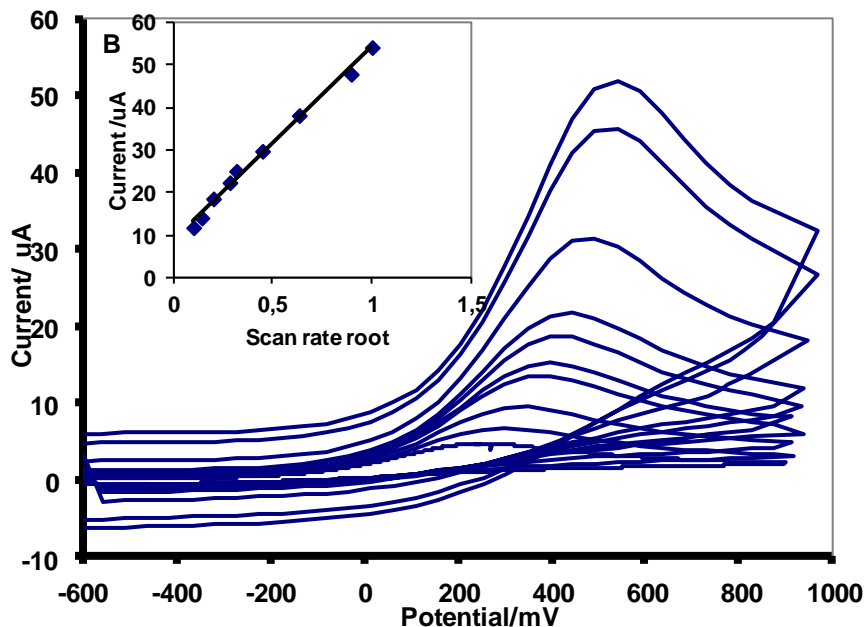


Figure 3. A) Cyclic voltammograms of 1.0×10^{-6} M OCA in 0.05 M BPS pH7.0 on (a) the bare GCE, (b) AuNPs /RGSN-IL/GCE; scan rate 200 mV/s; B) Typical Cyclic voltammograms of the sensor in 1.0×10^{-6} OCA 0.05 M PBS at different scan rates, 0.05, 0.1, 0.2, 0.4, 0.6, 0.8, 1.5, 2.0, 2.2 V/s

Fig. 3A showed the cyclic voltammograms of 1×10^{-6} M of OCA on GCE (curve a) and AuNPs /RGSN-IL/GCE (curve b) 0.05 M phosphate buffer solution at pH 7.0 at scan rate 50 mV/s. As shown, at the bare GCE OCA shows very weak redox peaks at potentials is about 450 mV and - 420 mV, which is an indication of the weaker adsorption reaction of OCA on the GCE surface. On the other hand, in this figure, the curve b shows a well-defined oxidation peak on the modified electrode, in which anodic a peak potential is about 420 mV, This indicates that the electrochemical process is catalyzed by the modified electrode. Therefore, it can be concluded that AuNPs /RGSN-IL/GCE could enhance the electron-transfer rate. In addition, it can be suggested that a larger number of OCA molecules reacts on the sensor surface, due to providing a larger area by nanocomposite.

Fig. 3B shows the typical CV curves of AuNPs RGSN-IL/GCE electrode in 1×10^{-6} OCA and 0.05 M PBS at different potential scan rates. It was seen that a large anodic peak appeared in the scan rate range from 0.1 to 2.2 V/s. As is shown a good linear relationship was found for the peak current and scan rate. The oxidation peak current rise proportionally with the linear regression equations as $i_p = 46.22v^{1/2} + 7.78$ ($R = 0.989$). This result suggests that the reaction is diffusion-controlled behavior with an electron transfer process.

Fig. 4 shows CFFTCV voltammograms and the changes in currents of the AuNPs/RGSN-IL/GC electrode in the potential range of -600 to 1200 mV in 0,05 M BPS at scan rate of 3 V/s. The time axis represents the time passing between the beginning of the experiment and the beginning of a particular sweep (i.e. it represents a quantity proportional to the sweep number) [14-17].

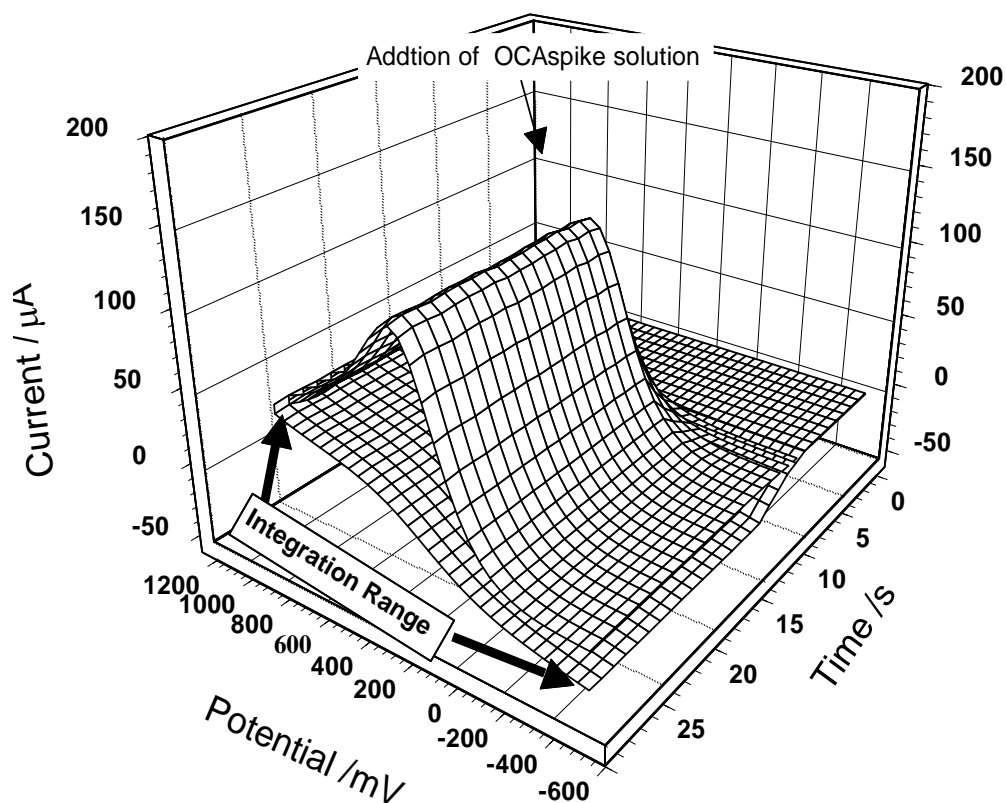


Figure 4. a) CFFTCV voltammograms of AuNPs/RGSN-IL/GCE in absent and present of 1.0×10^{-6} M OCA in PB solution at pH 7.0 in the potential range of -600 to 1200 mV at potential scan rate 3 V/s.

The potential axis on this graph represents potential applied to the working electrode during each potential scan. As can be seen, three dimensional presentation of the sensor response, provides more details about the effect of electrochemical reaction of OCA on currents of the CV by time, where more information can be obtained about the response time of the sensor.

The figure shows that there is no significant peak current in absent of OCA, but after addition of 2.0×10^{-6} M OCA in the BPS an oxidation peak appears at potential 520 mV. As mentioned above, the electrode response was calculated in form of the integration range for the ΔQ is -400 to 900 mV. However, as mentioned above the accumulation of OCA to high surface area of the sensor can enhance of direct electron transfer between the active sites of AuNPs/RGSN-IL/GC electrode. This can increase the peak current at the recorded voltammograms, when the OCA sample was spiked to the solution. For obtaining the best performance in the electrochemical measurement, the effect of the most important experimental parameters, such as the pH of the supporting electrolyte, amount of RGNS, the time of deposition of AuNPs and the potential sweep rate were examined and their values were optimized.

3.1. Optimization of sensor parameters

The dependence of the sensibility of the electrochemical method on the solution pH was studied over the range pH 5.0 to 8.0. Fig. 5 shows the changes of ΔQ (or the method sensitivity) for the oxidation current when the sensor was subject to 0.1 mM OCA solution at various pH PBS recorded at scan rate of 3 V/s. The results showed that at the pH values less than 7.0, the oxidation current increased steeply with the increase of pH, and then reached a maximum value at pH 7.0, and at higher pH the response decreased.

Fig 5 shows the results of examination of pH on the sensor response. However, from the graph, it can be concluded that the pH was increasing ΔQ was decreasing and oxidation potential was less positive, and the best pH chosen for the electrochemical measurements was around 7.0.

The relationship between the magnitude of AuNPs and different deposition time has been investigated. Fig 6 shows the effect amount of RGNS and the deposition time on the sensor response to 1.5×10^{-7} M OCA in 0.05 M PB solution at pH 7.0.

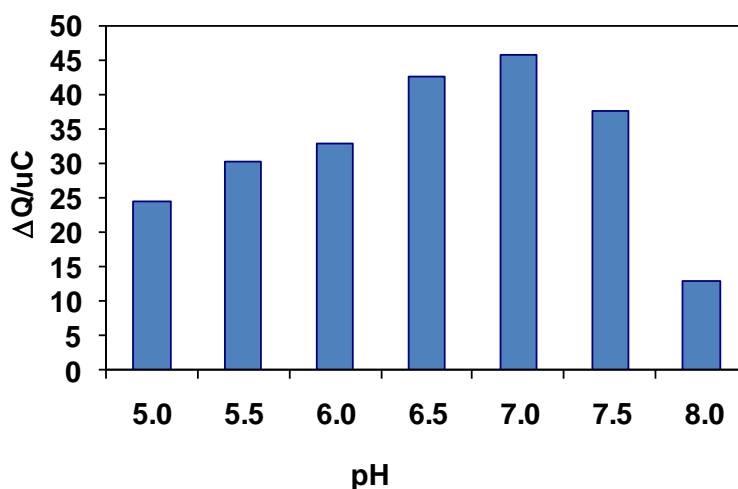


Figure 5. The effect of pH on the electrochemical response of AuNPs /RGNS-IL/GCE to 1.5×10^{-7} M OCA, in 0.05 M PB solution (the potential range of -400 to 900 mV at potential scan rate 3 V/s)

As shown in figure, the value of ΔQ increase with increasing amount of RGNS reaches to up to 4 mg the sensor response set at the maximum value. While at the higher amounts of RGNS the value of ΔQ decrease, which can be due to a higher surface resistance of the electrode surface. As a result, the best value for the amount RGNS in the modifier for sensor is 4 mg.

Moreover, dependence of the electrochemical detection method on the time of AuNPs deposition on the surface of RGNS-IL/GC electrode was investigated. As shown in the figure the sensor response initially increases with the time of deposition, up to 10 s and after that the sensor response slightly decreases.

It is well known that the morphology, magnitude and distribution of AuNPs, the amount of RGNS, can have influence on the performance of the sensor. It is reported that the deposition time, potential, and HAuCl_4 concentrations can control the magnitude and distribution of AuNPs. In fact, the time of depositions in this process control the size and mount of AuNPs on the electrode surface. Therefore, the optimum time for deposition for AuNPs was 10 s.

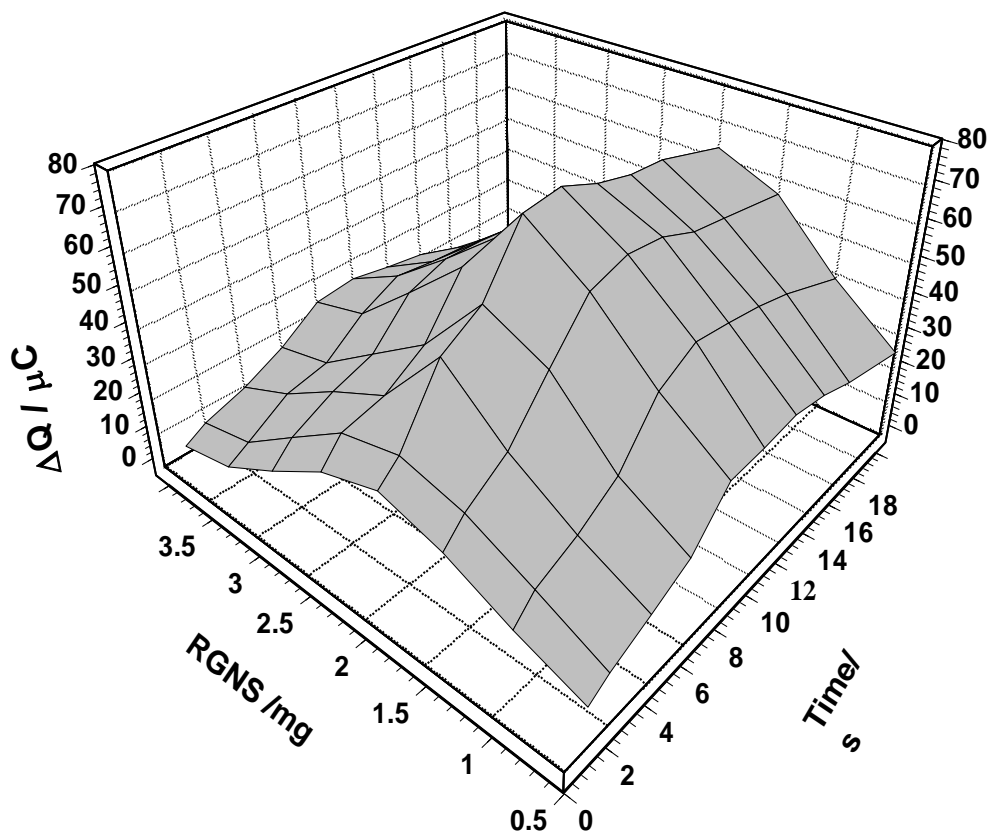


Figure 6. The effect of amount of RGNS and the time of deposition of AuNPs on the sensor response to 2.0×10^{-7} M of OCA in 0.05 M PBS at pH=7.0. The potential range of -400 to 900 mV at potential scan rate 3 V/s

3.2. Calibration curve

As mentioned above, in CF-FTCV measurements, the sensor response to OCA sample solution was calculated in form of C by integrating the current in a selected potential range around the oxidation peak. Therefore, the magnitude of the sensor response depends on the choice of the potential integration range. In order to obtain the best detection limits for the detection method, the important experimental parameters were set at optimum values. The results of that calculation for the sensor response are a curve in form of $Q(nC)$ vs. time.

The inset curve in figure 7 illustrates a typical ΔQ response for on standard solutions of OCA (from 2.0 to 30.0 nM in PB solution, pH 7.0, the potential range of -400 to 900 mV at potential scan rate 3 V/s). In this figure, each point represents the integrated signal for 3 consecutive additions of the

OCA standard solution. In general, the OCA response showed a linear dynamic range of 1.0 to 200.0 nM, A correlation coefficient of $R=0.997$ values. The detection limit, estimated based on signal to noise ratio ($S/N=3$), was found to be 2.2×10^{-10} M.

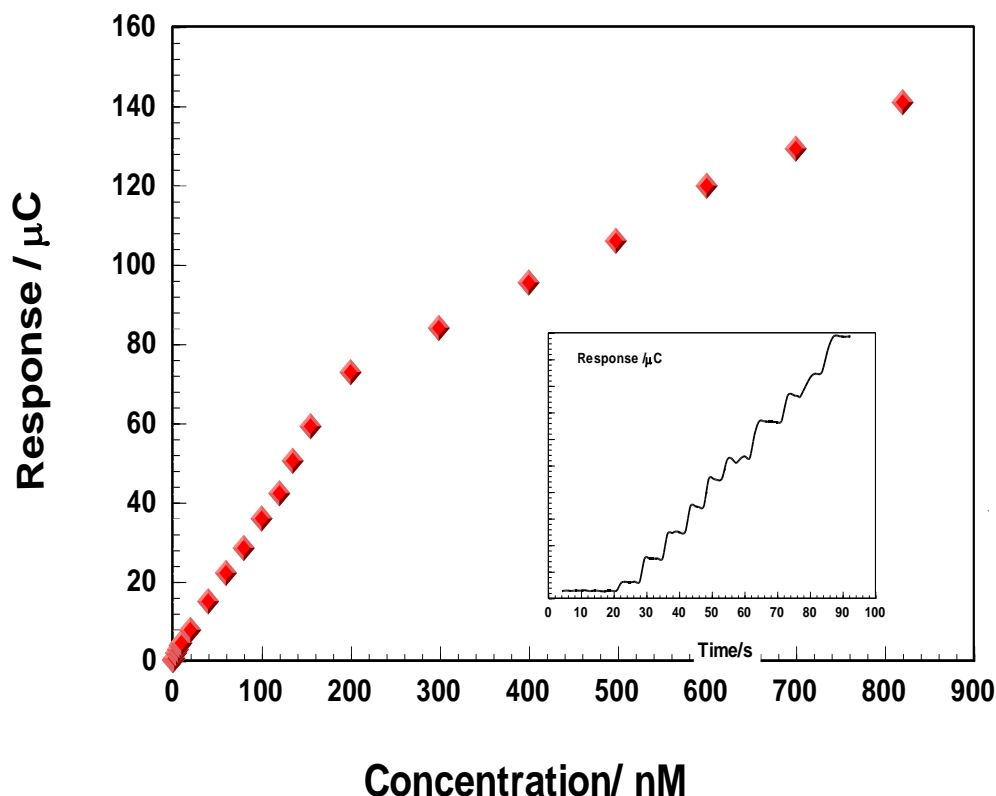


Figure. 7. The calibration curve for ochratoxin A determination, and the inset, response of the AuNPs /RGSN-IL/GC to OCA upon the following concentrations: a, 2 to 30 nM PB solution, pH 7.0. The potential range of -400 to 900 mV at potential scan rate 3 V/s.

The long-term storage stability of the sensor was tested for 60 days. The sensitivity retained 94.5% of initial sensitivity. It seems that the decline in the sensor performance after a long time of usage could be due to the loss of the materials on the surface of the sensor into the solution.

4. CONCLUSIONS

This paper presents, for the first time, a highly sensitive electrochemical detection method for determination of OCA. The new sensor was fabricated by AuNPs and RGNS hybrid with ionic liquid, on a glassy carbon electrode. It is seems that RGNS-IL coated can improve the sensing performance via factionalizing the graphene. The reason is the adsorption of OCA onto the planar surface of graphene oxide can reduce the concentration of OCA in the solution. For AuNPs /RGSN-IL/GC, the ratio of AuNPs and RGNS is very important for obtaining a better detection limit. By means of this method, it can be predicted that the detection limit of functionalized RGNS/AuNPs based sensing

platform can be decreased. Reproducible sensitivity response time less than 7 s was observed sensor (R.S.D value of 2.5%).

ACKNOWLEDGMENT

This work was supported by the research council of the University of Tehran.

References

1. L. Al-Anati, E. Petzinger, *J. Vet. Pharmacol. Ther.* 29 (2006) 79.
2. *Ochratoxin A Fact Sheet, Prepared for the U.S. Department of Agricultural Forest Service by Information Venture Inc.*, Copyright, (2005)
3. N.W. Turner, S. Subrahmanyam, and S.A. Piletsky, *Anal. Chim. Acta*, 632 (2009) 168.
4. S. Bräse, A. Encinas, J. Keck, and C.F. Nising, *Chem. Rev.*, 109 (2009) 3903.
5. IARC, International Agency for Research on Cancer (IARC), Some naturally occurring substances: food items and constituents, (IARC) *Monograph Evaluation of Carcinogenic Risk to Humans* No 56 (1993).
6. European Commission, *Off. J. Eur. Union* 364 (2006) 5.
7. European Commission, *Off. J. Eur. Union* 35 (2010) 7.
8. L. Afsah-Hejri, S. Jinap, and H. Mirhosseini, *Food Control*, 23 (2012) 113.
9. J.E. Welke, M. Hoeltz, H.A. Dottorib, and I.B. Nolla, *J. Braz. Chem. Soc.*, 21 (2010) 441.
10. G.J. Soleas, J. Yan, and D.M. Goldberg, *J. Agric. Food Chem.*, 49 (2001) 2733.
11. S. Almeda, L. Arce, F. Benavente, V. Sanz-Nebot, J. Barbosa, and M. Valcárcel, *Anal. Bioanal. Chem.*, 394 (2009) 609.
12. D. Flajs, A.M. Domijan, D. Ivic, B. Cvjetkovic, and M. Peraica, *Food Control*, 20 (2009) 590.
13. P. Norouzi, H. Rashedi, T. Mirzaei Garakani, R. Mirshafian and M. R. Ganjali, *Int. J. Electrochem. Sci.* 5 (2010) 377.
14. P. Norouzi, M. R. Ganjali, B. Larijani, A. Mirabi-Semnokolaii, F. S. Mirnaghi, and A. Mohammadi, *Pharmazie* 63 (2008) 633.
15. P. Norouzi, M. R. Ganjali, S. Shirvani-Arani, and A. Mohammadi, *J. Pharm. Sci.* 95 (2007) 893.
16. M. R. Pourjavid, P. Norouzi, and M. R. Ganjali, *Int. J. Electrochem. Sci.* 4 (2009) 923.
17. P. Norouzi, M. R. Ganjali, M. Zare, and A. Mohammadi, *J. Pharm. Sci.* 96 (2007) 2009.
18. P. Norouzi, M. Qomi, A. Nemati, and M. R. Ganjali, *Int. J. Electrochem. Sci.* 4 (2009) 1248.
19. P. Norouzi, B. Larijani, M. Ezoddin and M. R. Ganjali, *Mater. Sci. Eng. C* 28 (2008) 87.
20. M. R. Ganjali, P. Norouzi, R. Dinarvand, R. Farrokhi, and A. A. Moosavi-Movahedi, *Mater. Sci. Eng. C* 28 (2008) 1311.
21. P. Norouzi, M. R. Ganjali, and L. Hajiaghbabaei, *Anal. Lett.*, 39 (2006) 1941.
22. P. Norouzi, G. R. Nabi Bidhendi, M.R. Ganjali, A. Sepehri, M. Ghorbani, *Microchim. Acta*, 152 (2005) 123.
23. P. Norouzi, M. R. Ganjali, T. Alizadeh, and P. Daneshgar, *Electroanalysis*, 18 (2006) 947.
24. M. R. Ganjali, P. Norouzi, M. Ghorbani, and A. Sepehri, *Talanta*, 66 (2005) 1225.
25. P. Norouzi, M. R. Ganjali, and P. Matloobi, *Electrochem. Commun.*, 7 (2005) 333.
26. P. Norouzi, H. Rashedi, T. Mirzaei Garakani, R. Mirshafian and M.R. Ganjali, *Int. J. Electrochem. Sci.*, 5 (2010) 377.
27. P. Norouzi, F. Faridbod, E. Nasli-Esfahani, B. Larijani, M. R. Ganjali, *Int. J. Electrochem. Sci.*, 5 (2010) 1008.

28. P. Norouzi, F. Faridbod, B. Larijani, M. R. Ganjali, *Int. J. Electrochem. Sci.*, 5 (2010) 1213.
29. P. Norouzi, M. Pirali-Hamedani, F. Faridbod, M. R. Ganjali, *Int. J. Electrochem. Sci.*, 5 (2010) 1225.
30. P. Norouzi, M. R. Ganjali, A. Sepehri, and M. Ghorbani, *Sens. Actuators B* 110 (2005) 239.